OPEN ACCESS

Insights into the Path-Dependent Charge of Iridium Dissolution Products and Stability of Electrocatalytic Water Splitting

To cite this article: An Phuc Dam *et al* 2023 *J. Electrochem. Soc.* **170** 064504

Journal of The Electrochemical Society, 2023 **170** 064504

Insights into the Path-Dependent Charge of Iridium Dissolution Products and Stability of Electrocatalytic Water Splitting

An Phuc Dam,[1] Bassam Y. A. Abuthaher,[1] Georgios Papakonstantinou,[1] and Kai Sundmacher[1,2,z]

[1]*Max Planck Institute for Dynamics of Complex Technical Systems, Department Process Systems Engineering, Sandtorstr.1, D-39106 Magdeburg, Germany*
[2]*Otto-von-Guericke University Magdeburg, Department of Process Systems Engineering, Universitätsplatz 2, D-39106 Magdeburg, Germany*

The electrocatalytic stability of the oxygen evolution reaction (OER) is challenging for the storage of fluctuating renewable energies using polymer electrolyte membrane water electrolyzers (PEMWEs). Investigations are commonly conducted in so-called half-cell setups and different OER-related dissolution pathways have been proposed. However, the orders of magnitude difference in dissolution rate between half-cells and PEMWE using membrane electrode assemblies (MEA) is not well understood. In this work, the charge-related absorption affinity of Iridium (Ir) dissolution products, from both half-cell and MEA setups, is investigated, using cation and anion exchange materials. In the half-cell, a roughly constant ratio of cationic to anionic dissolution species is indicative of a single, dominant OER-related Ir dissolution pathway. While Ir dissolved in half-cells is mainly cationic, the Ir species from the MEA appear mainly in anionic form. This can be explained by the transport conditions of different Ir ions inside the catalyst layer, influenced by their ionomer absorption affinity and the migration driving force. Based on this understanding, key influences of electrocatalytic stability of MEAs, the effect of confinement of dissolved Ir species and the stability discrepancy to half-cells are discussed.
 [DOI: 10.1149/1945-7111/acd4f2]

Manuscript submitted December 20, 2022; revised manuscript received May 3, 2023. Published June 13, 2023.

Supplementary material for this article is available online

Polymer electrolyte membrane water electrolysis (PEMWE) is a key technology for energy storage of fluctuating, renewable energy sources. Due to the acidic environment and the high potential of the anodic oxygen evolution reaction (OER), so far only Iridium-based materials are suitable for application as electrocatalysts. However, it can be foreseen that the level of implementation of PEMWE will be limited by the scarcity of Iridium (Ir).[1–3] Therefore, drastically reducing catalyst loading, while maintaining efficiency and stability, is a key challenge. The degradation of the anode catalyst layer (ACL) becomes a severe problem at low loadings.[4–6] As the OER has an essential influence on both efficiency and stability of PEMWE, a lot of work has been dedicated in understanding the OER-related catalyst dissolution. So-called half-cell setups are commonly applied to investigate OER electrocatalysis. Liquid electrolyte is used in half-cells and typical configurations are the rotating disc electrode (RDE) or the scanning flow cell (SFC). The latter has been widely used, due to its ability to be coupled with inductively coupled plasma mass spectrometry (ICP-MS) and measure on-line Ir dissolution rates and assess the stability of different catalyst materials.

Different OER catalyst dissolution mechanisms have been proposed, depending on the surface type and the applied potential region. Ir complexes with different Ir oxidation states and ionic charges can occur as a result of different dissolution processes.[7–9] A dissolution path via Ir oxidation state +6 (IrO_4^{2-}) was proposed to occur at higher potentials with crystalline surfaces,[7,8] whereas dissolution of Ir^{3+} was suggested at lower potentials on more amorphous surfaces.[10] Based on investigations using isotope labelling it was suggested that lattice-oxygen participation is a key mechanism that leads to both higher OER activity and lower stability of Ir oxides.[11] To the best of our knowledge, it has not yet been tested, if this proposed fundamental mechanism is supported by the characteristics of the dissolved Ir species. Furthermore, the relative fraction or significance of different dissolution pathways has not been quantitatively evaluated.

The so-called stability-number has been introduced as a metric to compare different OER catalytic materials. With the definition $S_{num} = \frac{n_{OER}}{n_{Ir}}$, the stability-number measures how many moles of oxygen a specific surface produces per Ir atom dissolved. Beside the comparison of different catalyst surfaces, the introduction of the stability-number has also emphasized the large difference between the half-cell setup and the applicational PEMWE cell, in which a membrane electrode assembly (MEA) is utilized. It has been reported that the steady-state stability-number evaluated in the anode water effluent of PEMWEs is four orders of magnitude higher than in half-cells.[12,13] Therefore, it becomes clear that the analysis of this discrepancy can be of essential importance to understand electrocatalytic stability in PEMWE. Recently, Geiger et al.[12] and Knöppel et al.[13] have provided valuable insights into the discrepancy question. Based on the observation that the OER onset potential is ca. 100 mV higher when the PEMWE anode is fed with 0.1 M H_2SO_4, Knöppel et al. suggested that the local pH of PEMWE ACL is higher than it has been usually assumed. Furthermore, operating the MEA with 0.1 M H_2SO_4 and 0.1 M $HClO_4$, instead of pure water, leads to two and one order of magnitude lower stability-numbers, respectively. However, a decrease in acidity from pH = 1 to pH = 3 in the SFC decreased the dissolution rate by only a factor of 3.3.[13] Thus, the key influences in the discrepancy between dissolution in half-cells and PEMWEs are still an open question.

In this work, the properties of Ir corrosion products formed under different electrochemical dissolution conditions in RDE half-cells and PEMWE MEA setups are investigated by systematically studying the interaction with cation and anion exchange materials at different acidity levels of the liquid phase. The aim is to gain insights into characteristics of the dissolution products and related consequences for their transport characteristic. Based on that, implications on the mechanistic nature of Ir catalyst dissolution during OER and essential influences for the understanding of electrocatalytic stability of PEMWE can be discussed. The role of particle detachment in Ir loss from MEAs is assessed. Dissolved Ir species from different setups (MEA and half-cell), electrochemical protocols (static and dynamic) and Ir surface types (Ir metallic, IrOx-

[z]E-mail: sundmacher@mpi-magdeburg.mpg.de

nano-particles) are studied. The ionic form (anionic/cationic) of the dissolved complexes is of particular interest, due to its role in the transport of the dissolved species and the absorption and migration behavior in the ACL ionomer phase. Implications on the understanding of electrocatalytic stability of PEMWE are discussed based on the analysis of mass transport, thermodynamics and key observations of Ir dissolution. Additionally, the option of catalyst recovery from the anode water of PEMWE is discussed based on the observed absorption characteristics of the Ir dissolution products.

Experimental

Ir-containing solutions from the half-cell.—A schematic summarizing the overall procedures is shown in Figure 1. The Ir dissolution process in the half-cell was performed with a rotating disc electrode (RDE) setup, area 0.196 cm^2, with a rotation rate of 750 rpm in 125 ml of 0.1 M $HClO_4$ electrolyte in a glass cell. To avoid bubbles, sticking centrally to the working electrode (WE) despite rotation of the WE, an external PTFE stirrer was fixed close to the RDE tip. A Hydroflex® reference electrode (RE) was used inside a glass capillary. As the counter electrode (CE) a platinum mesh was placed inside a tubular PTFE compartment, separated from the main solution by a Nafion 115 membrane. An Autolab PGSTAT302N potentiostat (Metrohm) was used to perform the electrochemical polarizations.

IrOx nanoparticles.—To obtain a good anchorage on top of the Au RDE tip, the latter was roughened with a 15 μm diamond suspension. To prepare the catalyst suspension, IrOx (Alfa Aesar, Iridium(IV) oxide, Premion, 43396) was dispersed in a solution of 20 vol% isopropanol and 80 vol% water. Proper mixing was ensured by 10 min bath sonication and 30 s horn sonication. The target loading of 50 μg IrOx cm^{-2} was obtained by drop-casting 10 μl of the suspension on top of the Au tip, which was then left to dry at 200 rpm at ambient conditions. After that, 5 w% ionomer suspension (Liquion, IonPower) was diluted with a 1:1 vol. water-isopropanol mixture and sonicated for 15 min. 10 μl of the resulting suspension was drop-casted on top of the catalyst film, preheated by an infrared lamp to ca. 60 °C, in order to provide an ionomer loading of 10 w% with respect to the catalyst loading. The ionomer was drop casted atop, in order to achieve higher catalyst utilization by avoiding blockages of the electron percolation pathways to and from the conductive substrate,[14] which may occur at high ionomer loadings with catalyst-ionomer mixtures.[15] In two of the obtained Ir-containing solutions, the dissolution process was conducted galvanostatically either at lower (4 mA cm^{-2}, "lcd") or higher current density (15 mA cm^{-2}, "hcd"). An additional dissolution protocol with IrOx nanoparticles contained potential sweep below and within OER potentials (Fig. S2).

Ir tip.—The Ir tip was polished using a 1 μm diamond suspension. Cyclic voltammetry below OER onset was used to make sure that the surface shows the typical features of metallic Ir initially after polishing. Before the actual OER dissolution procedures, the WE was anodically polarized at 2 mA cm^{-2} in a separate solution of 0.1 M $HClO_4$ for at least 1.5 d to ensure a well-defined oxidized surface on the Ir tip. Under these conditions it can be expected that a thin hydrous Ir oxide layer on top of a compact oxide layer is formed.[16] With the Ir tip three different Ir-containing solutions were produced. Two of them were created under OER conditions. In the low current density case ("lcd"), a constant current density of 2 mA cm^{-2} was applied for around 70 h. In the high current density case ("hcd"), an average current density of ca. 36.4 mA cm^{-2} was applied (Fig. S3) for ca. 110 min. For the third Ir tip solution, Ir was dissolved from a metallic state of the Ir tip (right after polishing) via voltammetric cycling between 0.04 V and 1.2 V. The applied cycles were: 600 cycles with 200 mV s^{-1}, 72 cycles with 50 mV s^{-1} and 43 cycles with 200 mV s^{-1} sweep rate.

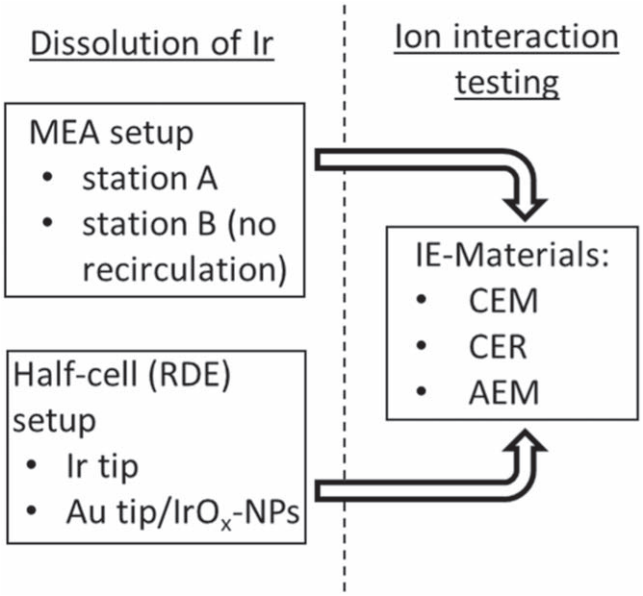

Figure 1. Summarizing schematic of experimental procedures from dissolving Ir under different electrochemical conditions towards testing of Ir ion interaction with different ion exchange (IE) materials.

Ir-containing solutions from PEMWE.—The anode water effluent of PEMWE single-cells was collected from two different test stations (A and B) with different electrochemical protocols. In test station A, a circular Ti cell (active area of 63.5 cm^2) and a catalyst coated membrane (CCM) from Ion Power GmbH were used. The latter consists of a Nafion 117 membrane, an Ir-based anode and a Pt-based cathode. CCM of the same batch was physicochemically characterized in Ref. 17. A Ti felt (Bekaert, 1 mm thickness, 75% porosity) was used as anode porous transport layer (PTL). A hydrophobized carbon paper (H2315 I6, 210 μm thickness, Freudenberg), along with a woven carbon cloth (700 μm, Sylatech Analysetechnik) was used on the cathode side. A Ti micro-grid expanded metal (7 Ti 10–050, 0.9 mm thickness, Dexmet) served as anode spacer to allow for efficient mass transport. The water was recirculated via tubes and a water tank, which are made of stainless steel. Tests were conducted with a FuelCon commercial test station. A Solartron 1287 A potentiostat and a 1250 B frequency response analyzer were connected in parallel to the single cell and the 2-quadrant load (0.03–100 A, FuelCon). The electrochemical procedure of test station A contained cyclic voltammetry at the beginning and the end of a constant cell potential (1.8 V) operation for 132 h at 60 °C (average current density ca. 1 A cm^{-2}). Cyclic voltammetry was performed between 0.5 V and 1.35 V at different sweep rates (1 − 30 mV s^{-1}). The water was collected from the anode tank after operation (schematic Fig. S1a).

A rectangular cell with active area of 70 × 35 mm^2 (ca. 25 cm^2) was used in test station B. The CCM (Ion Power GmbH), consisted of a Nafion 117 membrane with an Ir loading of 0.5 mg cm^{-2} (IrOx Alfa Aesar, 43396) and an ionomer fraction of 0.21. Pt loading on the cathode side was 0.2 mg cm^{-2}, with an ionomer fraction of 0.25. A Pt-coated Titanium felt (Bekipor®, Bekaert, uncompressed thickness and porosity of 1 mm and 77%, respectively) served as PTL. The flow field is made of Ti. Tubing, pumps and water tank are made of plastic or PTFE. For the electrochemical experiments, an AMETEK Solartron Analytical EnergyLab XM ECS potentiostat was used in combination with a 20 A Booster. The cathode side was operated at ambient pressure and fed with 50 ml min^{-1} H_2 to ensure well-defined cathode conditions and potential. Before the dissolution procedure, the system was stabilized by six up and down sweeps between open circuit potential and 1.8 V and a constant galvanostatic operation at 0.68 A cm^{-2} for 8.5 h. Ir was dissolved during

galvanostatic OER operation at different cell inlet temperatures (room temperature and 0.68 A cm^{-2}, 40 °C and 0.68 A cm^{-2}, 60 °C 0.8 A cm^{-2}). In case of test station B, sampling of the Ir-containing water was conducted during operation directly at the anode outlet of the cell, which was fed from Temperature-controlled external source of Ir-free water, thus, without recirculation (schematic Fig. S1b). Before collecting the Ir-containing water of the different operating points, the system was given 40 min to stabilize under the same constant polarization conditions. The flow rate during sampling of Ir-containing water was 20 ml min^{-1}.

Absorption testing of Ir dissolution products.—After completing the different Ir dissolution procedures, absorption tests with the Ir containing solutions were performed in separate beakers. The interaction of the Ir dissolution products was tested with different ion exchange (IE) materials: Cation exchange membranes (CEM, Nafion 117, Quintech), cation exchange resins (CER, MonoPlus SP 112 H, Decker, delivery form H^+) and anion exchange membranes (AEM, Fumion FAA-3–30, Fumatech, delivery form Br^-). Nafion 117 was pre-treated in 5% H_2O_2, 1 M H_2SO_4 and water, in the mentioned order and each for 2 h at 80 °C. The AEMs were pre-treated by immersing in 1 M KOH overnight and then in H_2O overnight to exchange the Br^- with OH^-. The volume of the solutions for the absorption tests was 25 ml. The size of the membranes used for absorption testing was 2.4 × 2.4 cm^2 and the amount of resin was 0.7 g, if not specifically mentioned differently. Iridium was quantified using inductively coupled plasma mass spectrometry (ICP-MS, PlasmaQuant MS Elite, Analytik Jena). A 5-point calibration (3, 1, 0.1, 0.05, 0 [blank] ppb) was performed before each measurement series. A standard solution was measured after ca. every three sample analyses to detect and correct possible drifts of the signal. After immersion of an ion exchange membrane, the diffusion-controlled absorption process takes ca. 100 h to equilibrate (Fig. S4). The absorption process is faster in the CER case. Finally, the absorption fraction, defined as absorbed amount of Ir to the initial amount of Ir in solution, was measured after ca. 9 d of immersion.

Results and Discussion

Iridium dissolution products from half-cell.—Figure 2 shows the absorption fractions of dissolved Ir, obtained via different half-cell setup procedures in the cation exchange resin (CER). The top line of the columns shows the model-corrected data, which accounts for the amount of Ir already absorbed during the dissolution process (model details in supporting information) in the small Nafion CE-separator. It can be seen that the model-based corrections are very small or negligible due to the small separator membrane size and the relatively short dissolution procedures (Fig. 2). A roughly constant fraction of around 80% is absorbed for Ir-containing solutions obtained via OER polarization. The sweeping protocol with a metallic Ir below OER potentials resulted in a higher absorption fraction of ca. 90%.

The absorption in the case of the cation exchange membrane (CEM) is slightly less (Fig. S5), however, both experiments with CEM and CER suggest that the majority of dissolved Ir species is of cationic type. Ir^{3+} can be considered as the main contribution of the absorbed cationic species for both dissolution during OER[7,10] and potential sweeping below OER potentials.[9,18] The small fraction of Ir, which is absorbed in CER but not in CEM, may be attributed to a second cationic Ir species with lower absorption affinity. This is supported by the observation that, after dilution with water, the absorption fraction in CEM attains a similar level with that in the CER (Fig. S8). It may be hypothesized that there is another cationic species that does not fully absorb in CEM under highly acidic conditions. A hydrated, dissolved form $Ir(H_2O)_6^{3+}$ has been reported in the literature.[10,19]

The reason for the non-absorbed fraction shall be further investigated. Absorption/desorption of metal ions in materials can typically be described by a partition coefficient $K_p = \frac{c_{mem}}{c_{sol}}$.[20,21] Two hypotheses are discussed: (1) The absorption fraction is established by one type of Ir species, which reaches equilibrium as a result of the intrinsic partition coefficient. (2) There is an occurrence of one (or more) other type of Ir species and the observed total absorption fraction is the result of the individual partition coefficients. The affinity can be expected to be strongly influenced by the ionic form (cationic/anionic) of the Ir complex.

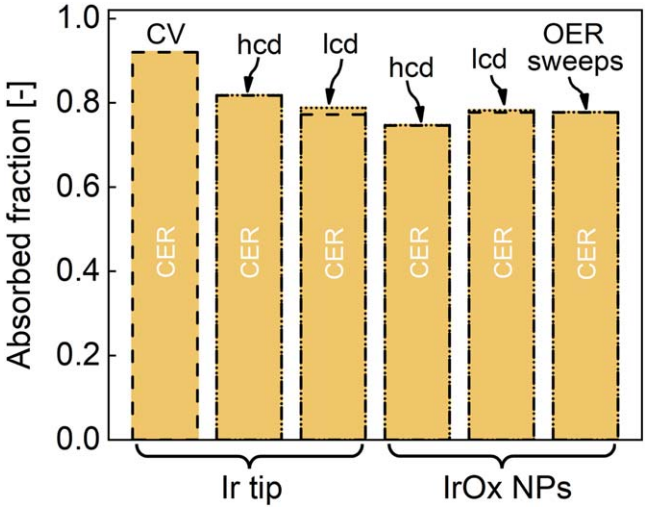

Figure 2. Absorption fraction of Ir in CER. Ir was dissolved in the RDE setup, either from an Ir tip or IrOx-nanoparticles. "hcd" and "lcd" denote high and low OER current density, respectively. The dashed lines represent the as measured values. The dotted lines account for Ir cations already absorbed in the small CE-separator membrane during the half-cell dissolution process, showing that this influence is almost negligible (more modelling details in the supporting information section 3.1).

Different experimental observations indicate that hypothesis (1) is not a suitable explanation. Figures S6 and S7 show the negligible dependence of the absorption fraction on the quantity of ion exchange materials (ten times more CER material or half the CEM size), which is against hypothesis (1) of an equilibrium of one type of species and its partition coefficient. The theoretical, maximum capacity of the ion exchange materials is certainly not reached since it is much higher than the amount of dissolved Ir in the solutions. Based on the ion exchange capacity (1.35 meq g^{-1}) and the weight of the used CEM, the amount of ion exchange sites exceeds the Ir amount in solution by ca. a factor $2{\cdot}10^6$. Furthermore, as a consequence of hypothesis (1), the absorption of Ir would be influenced by the competition with the absorption of protons. However, decreasing proton activity by factor 100 leads to only a small absorption increase in the CEM and negligible change in the CER case, as can be seen in Fig. S8.

Meanwhile, the absorption fraction is independent of the initial Ir concentration (Fig. 3), when maintaining a constant proton activity by diluting with the same 0.1 M $HClO_4$ solution. However, by testing the remaining Ir fraction via replacing the "used" ion exchange materials with "new" ones, one can see that the absorption fraction of the second absorption step is either negligible (for CER) or much smaller (for CEM). These findings suggest that the remaining Ir fraction is a different type of species than the absorbed ones. Therefore, (at least) two significant fractions of different Ir species have been created in the preceding OER Ir dissolution process with one of the fractions showing a very low affinity for absorption in cation exchange materials. Since changing the absorption competition with protons by diluting 100 times with water or with 0.1 M $HClO_4$ does not change the non-absorbed fraction of ca. 20% (Figs. S8, 2 and 3), the non-absorbed species unlikely correspond to a cationic species with lower absorption affinity than protons, but rather an anionic Ir complex can be suggested.

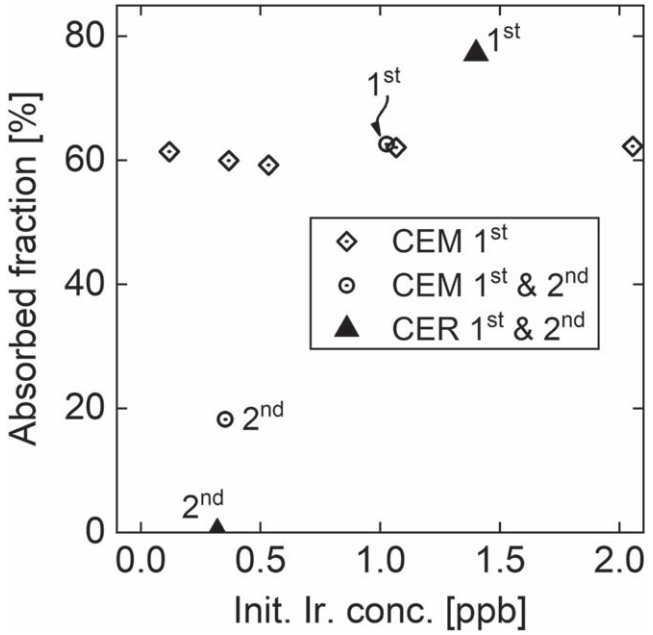

Figure 3. Observed absorption fractions in CEM and CER. Ir dissolved during OER at low current density (2 mA cm^{-2}) with an Ir tip. For the diamond symbol data ("CEM 1st") the initial concentration before immersing the CEM was varied by dilution with the same 0.1 M $HClO_4$ solution. Two consecutive absorption steps were conducted for the experiments labelled with "1st & 2nd." For the second absorption step, after the first absorption step, the "used" ion exchange material was replaced by new ion exchange material. All absorption fractions shown here are calculated with respect to the concentration of the solution directly before immersing the ion exchange material of each individual absorption step. The x-axis refers the initial concentration of each individual absorption step.

Different anionic complexes, such as $Ir(OH)_6^{2-}$ or IrO_4^{2-}, have been proposed in the literature, however, determination of the precise nature of these Iridium species is challenging.[22,23] It is noted that absorption tests were performed also with AEMs. Without dilution with water, a negligible Ir absorption fraction is observed, due to the competition with perchlorate anions, which occupy the AEM sites (Figs. S10 and S11). On the other hand, with 100 times water dilution, both cationic and anionic fraction are almost fully absorbed, the former due to the reaction given by Eq. 1. The reaction is well-known to occur in basic conditions above a transition region between pH 12 and 14.[24,25] Based on the ion exchange capacity (IEC) of the AEM, a local pH of 14.6 can be estimated.

$$Ir^{3+} + 6\,OH^- \rightleftharpoons Ir(OH)_6^{3-} \quad [1]$$

Different dissolution pathways during OER have been proposed.[7,8,11] A superposition of pathways would lead to a strong potential/current dependence, unless the two pathways are "coincidentally" characterized by very similar potential dependence, in particular, a very similar reaction rate vs potential slope, in mV per decade. Depending on the microkinetic structure of the dissolution reaction path, a large variety of electrochemical dissolution reaction slopes can occur for different pathways.[26] Different dissolution procedures with orders of magnitude difference in dissolution rates (factor 11.1 for IrOx-nanoparticles and 227 for Ir tip between "lcd" and "hcd" case), different Ir oxide surface (Ir tip vs IrOx-NPs) and ways of polarization (steady-state vs dynamic sweeping) have been applied to obtain the Ir-containing solutions for absorption testing. The observation that, despite the significant differences in the dissolution procedures, the observed fraction of anionic Ir species is roughly constant at around 20% is indicative of a single, dominant Ir dissolution pathway under OER conditions. It can be hypothesized that this dissolution pathway is related to the destabilization and disruption of the lattice structure, due to lattice oxygen participation during OER,[11] which leads to the observed constant fraction. In the following sections, the influence of the ionic properties of Ir species on the characteristics of their transport in PEMWEs, as well as the macroscopic effect on electrocatalytic stability are discussed.

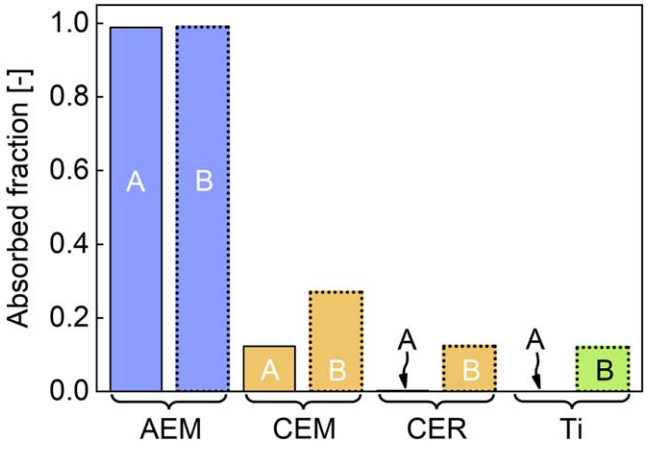

Figure 4. Absorptionfraction of Ir dissolved from the anode side of the MEA setups. "A" and "B" refer to the Ir-containing PEMWE anode water effluents, which were obtained via the dissolution procedures performed with test stations A and B, respectively. In test station B, galvanic displacement was minimized by the use of plastic materials, noble metal coatings and a flow-through mode without recirculation. The results of additional Ir deposition tests on a Ti plate are also shown.

Iridium dissolution products dissolved from PEMWEs.—Firstly, in order to quantify a possible influence of nanoparticle detachment, ultracentrifugation was conducted with the Ir-containing solution obtained from the PEMWE anode water tank. An average relative centrifugal force (RCF) of 142500 was applied. Assuming spherical particles and a underestimating guess of 2 nm diameter, Stokes law predicts a nanoparticle transport distance of 5 cm within 2 h. Centrifugation was performed for 16.8 h. Based on Transmission Electron Microscopy observations,[17,27] the considered 2 nm is an underestimation of the particle sizes to ensure that enough time is given for the separation of small particles, if present, since they will sediment slower. After centrifugation, samples were taken with a pipette from the top of the centrifugation tubes. Figure S12 shows that ultracentrifugation had no significant effect on measured Ir concentration, indicating that nanoparticle detachment is a negligible mechanism in the loss of Ir in PEMWE, provided that the MEA is well-fabricated.

The results of absorption experiments with Ir-containing water effluent from the anode of the two MEA setups are shown in Fig. 4. In contrast to absorption tests of Ir from the half-cell, the cation exchange materials show either no or only small absorption fractions. On the other hand, Ir dissolved from the PEMWEs is almost entirely absorbed by AEMs. These observations together indicate that, in contrast to the Ir species dissolved in half-cell experiments, the dissolved Ir species of the MEA setup are mainly of anionic type. It is noted that this different absorption behaviour is not due to the acidity difference to the half-cell electrolyte. As one may expect, addition of acid to the Ir-containing water from the MEA setup results in even slightly lower absorption in the cation exchange materials (Fig. S11).

Small differences are observed in absorption between the solution from test station A and B, which can be explained by the different materials and procedures applied. In test station A, the water was recirculated in a system with many stainless-steel parts. Galvanic displacement takes place, e.g. via reaction $2\,Ir^{3+} + 3\,Ti \rightleftarrows 3\,Ti^{2+} + 2\,Ir$ already during the electrolysis experiment,[13,28] which also explains why negligible absorption of Ir on metal surfaces can be observed in absorption tests afterwards (Fig. S19). On the other hand, plastic materials and a Pt-coated PTL were used in test station B to prevent galvanic displacement of

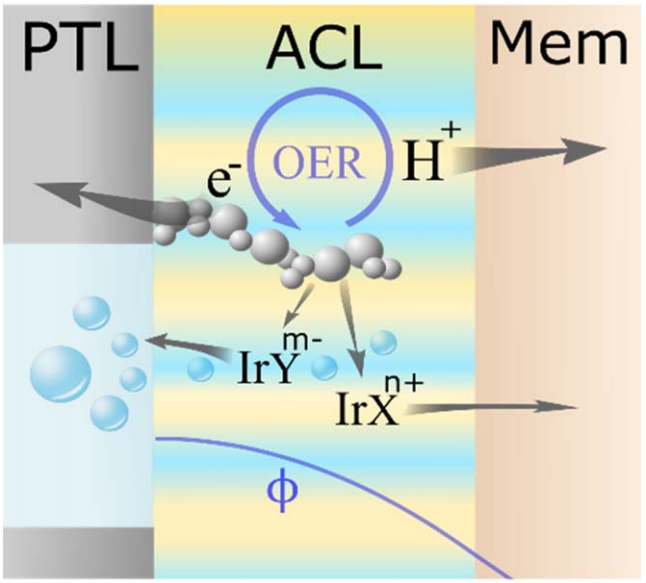

Figure 5. Schematic representation of ion transport in the PEMWE anode catalyst layer either via ionomer or water phase, insinuated by a yellow and blue colour, respectively.

dissolved Ir. Furthermore, in test station B, single pass water was sent into the cell and collected directly at the cell outlet without recirculation. The reduced galvanic displacement in the system, in turn, leads to a higher remaining fraction of cationic Ir.

The difference between the ionic forms of Ir species in half-cell and MEA setup can be understood considering the transport conditions of dissolved Ir in the ACL structure. Cationic Ir species have a high affinity to be absorbed inside the ACL ionomer phase. Therefore, they are not expected to be significantly affected by the vigorous bubble-induced mixing of the liquid phase. Instead, they are influenced by the migration driving force, which is directed towards the membrane side of the ACL. On the other hand, anionic Ir species are dissolved in the water phase of the ACL, as schematically illustrated in Fig. 5. Even though the net flow of water is directed towards the membrane direction, vigorous O_2 bubbling leads to strong intermixing of the liquid phase. Consequently, there is an effective transport of the dissolved, anionic Ir species to the channel direction, also supported by the driving force of migration. Therefore, the transport conditions result in the accumulation of anionic Ir species in the PEMWE anode effluent water.

It is noted that, in addition to the effect of mass transport conditions, also a change in the dissolution mechanism inside a PEMWE ACL, compared to the half-cell, may be a possible influence for an increased anionic Ir fraction. From a thermodynamic point of view, the local pH in the MEA ACL could favour anionic species. This can be seen in the Pourbaix diagram of Iridium, in which the operating point moves closer to the equilibrium line of IrO_2/IrO_4^{2-} with an increase in pH (see Fig. 7). A similar tendency can also be observed with a temperature increase. By varying the inlet temperature of the water fed into the PEMWE cell, indeed, the cationic fraction was observed to decrease with temperature, however, the influence was very small (Fig. S13). The interaction with fluorides (IrF_6^{2-} or IrF_6^{3-}),[17,29] which could be possible membrane degradation products, appears of less importance. Thermodynamic considerations suggest that, due to the low fluoride concentrations, non-fluoride involving dissolution products Ir^{3+} and IrO_4^{2-} are more favourable (see supporting information section 4).

Closing the balance of dissolved Ir in the MEA setup is challenging, due to the difficulty of reliably quantifying the amount of dissolved Ir transported into the membrane directio, as Ir can be both in ionic or deposited, solid form in different areas of the MEA, which is neither homogeneous nor void-free. An estimation shall be conducted based on the 27% cationic fraction found at the anode cell outlet of test station B (Fig. S13) and the assumptions that (1) a similar fraction of ca. 80% of dissolved Ir are cationic (Figs. 2 and S8) as in the half-cell case, and that (2) anionic Ir is fully transported to the PTL direction. One can then calculate that only ca. 9% of the dissolved cationic Ir is transported through the PTL direction to the flow channel. Ca. 27% of Ir ions are transported to the PTL direction, whereas 73% are either transported further into the membrane or remain in the ACL. Consequently, based on these considerations, the total stability-number corresponding to the total amount of dissolved Ir can then be estimated by the stability-number observed from sampling Ir concentration in the anode water channel via $S_{num,tot} \approx \frac{S_{num,ch}}{3.7}$. It should be noted that redeposition of the accumulated dissolved cationic Ir species in the ACL, can lead to an increase of the effective stability-number, which will be part of the discussion in the following section.

Accumulation of dissolved catalyst in ACL and electrocatalytic stability of OER.—As mentioned in the introduction, different influences on the discrepancy in stability-numbers between half-cell and MEA setups have been proposed. In this section, the effect of accumulated concentration on the electrocatalytic stability is

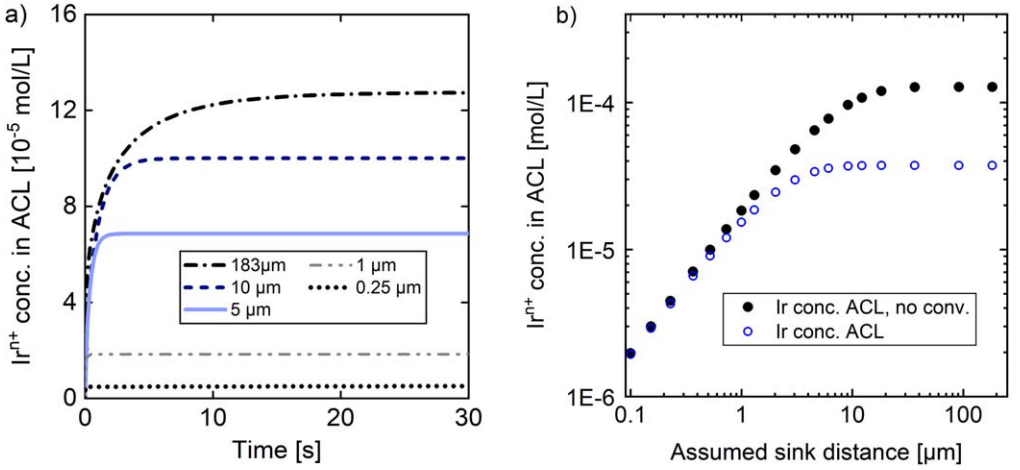

Figure 6. (a) Studying the confinement of Ir species via dynamic simulation of accumulation of cationic Ir species within the ionomer phase of the PEMWE ACL depending on the assumed sink distance. (b) Simulated steady-state concentration of cationic Ir species inside the PEMWE anode catalyst layer at 2 A cm^{-2}, depending on the assumed sink distance. For the hypothetical case study simulation, the IrOx dissolution kinetics are taken from experiments in half-cells without considering any effect of dissolved Ir concentration. Simulations with and without the convection term of the Nernst-Planck-equation are shown.

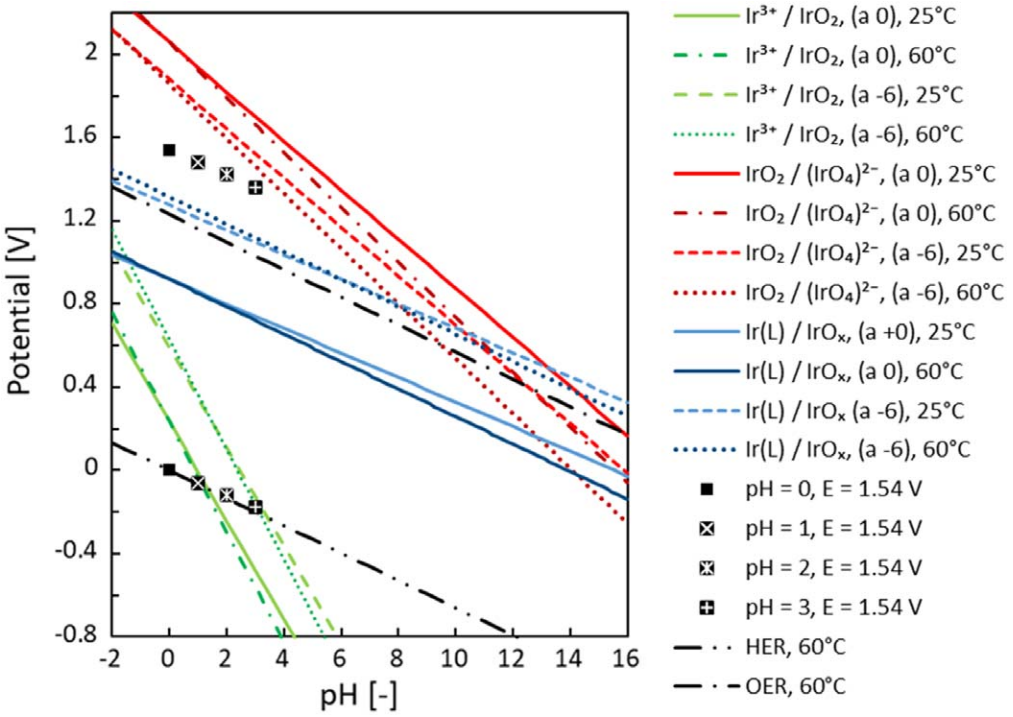

Figure 7. Pourbaix diagram of Iridium[9], calculated for 25 °C and 60 °C. The symbols represent the PEMWE anode catalyst layer (upper) and cathode catalyst layer (lower) operational points, depending on the assumed pH. A value of 1.54 V is chosen as a possible, typical iR-free potential. The added blue lines represent a thermodynamic dissolution/redeposition reaction equilibrium, which was more recently suggested in the literature.[23] "a −x" corresponds to a ratio of 10^{-x} for the activity of the dissolved Ir species over the activity of the undissolved Ir.

discussed. This concentration effect can have an influence on stability in two different ways: Firstly, the redeposition of dissolved Ir on nanoparticles in the ACL and, secondly, the effect of change of the driving force for dissolution (Nernst-potential), which decelerates the dissolution process in the first place. In the following, such a concentration effect will be analyzed from a mass transport and thermodynamic point of view as well as via comparison to key observations of Ir dissolution made in half-cells and MEAs.

Model-based analysis mass transport of dissolution products.—A mathematical model was developed to obtain insights on the transport confinement of Ir cations related to the PTL/water and membrane boundary conditions and possible, resulting accumulation levels of dissolved Ir species. The hypothetical scenario shall be reflected that there is no redeposition and the intrinsic stability-number of the process is similar to values, which can be observed in the half-cell setup. The following model assumptions were considered: (1) Stability-number typical for IrOx in half-cells. (2) No concentration effect is considered. (3) The ACL is considered zero-dimensionally, the membrane one-dimensionally. (4) Ir cations dissolving within the ionomer phase and their transport is described by the Nernst-Planck equation. (5) Due to the affinity of Ir cations to stay in the ionomer phase, the flux of the cationic Ir species to the PTL direction is much lower than the flux into the membrane direction and can therefore be neglected. The model equations and more detailed explanations about the derivation and assumptions of the model can be found in the supporting information section 3.

A 100% sink of the Ir ions is considered and its distance to the ACL is varied in the different simulations, which mainly influences the transport mode of diffusion. One may for instance assume the deposition to occur at the cathode side ($d_{sink} \approx 183\,\mu m$ for a Nafion 117 membrane) or much closer to the ACL at the frequently observed "Ir band," a few tenths of μm away from the ACL.[6,17] Figure 6b shows the simulated Ir cation concentration in the ACL over time. The steady-state concentration is reached fast. For assumed sink distances above 10 μm, diffusion does not play a significant role (Fig. 6a) and the steady-state concentration is reached within ca. 20 s (Fig. 6b). Steady-state is reached even faster with a shorter sink distance. Figure 6a shows the accumulated steady-state concentration in the ACL. For a sink distance of 0.25 μm, which corresponds to a typical location of the experimentally observed "Ir band,"[17] the steady-state concentration level is ca. $6.5 \cdot 10^{-6}$ mol l^{-1}. When the sink distance is assumed higher than 10 μm, which is plausible as a significant portion of dissolved Ir appears to arrive at the cathode side,[5,6] the calculated Ir concentration without convection term is ca. $1.3 \cdot 10^{-4}$ mol l^{-1} (Fig. 6a). From the two simulations, the one without consideration of the convection term seems more applicable, since the Ir cations are not dissolved in the water phase, but are rather adsorbed on the fixed sites of the membrane.[30] In both cases the concentrations are very high compared to those typically measured in half-cells, which are below 10^{-9} mol l^{-1}.[11,13] It is noted that, due to the zero-dimensional consideration of the ACL, an average concentration value is estimated. A concentration distribution within the ACL leads to even higher local concentrations at the reactive interfaces. This demonstrates a strong confinement of dissolved Ir species inside the ACL of the MEA setup, which may lead to important effects on catalytic stability as will be discussed in the following sections. Furthermore, this implies that it would be difficult to test the effect dissolved Ir concentration levels on the dissolution or possible redeposition rate inside the half-cell. The reason is that e.g. by purposely introducing such high concentrations of dissolved Ir species into the electrolyte, the relative measurement error of quantification (e.g. by ICP-MS) becomes too high and, consequently, masks the effect of the relatively slow dissolution and redeposition rates.

Thermodynamics of dissolution and redeposition.—As mentioned before, the accumulation of Ir can affect the measured stability-number as it can lead to redeposition or to a decreasing driving force and dissolution rate in the first place. Redeposition can occur via chemical reaction, possibly also related to H_2 permeation, or via electrochemical reaction. The thermodynamic driving force for the latter can be understood from the Pourbaix diagram of Ir. Figure 7 shows the thermodynamic equilibria calculated for conditions under

typical PEMWE operation. It can be seen that under OER potentials, there is a large overpotential of Ir^{3+} for the electrochemical reaction to IrO_2, depending on the assumed local pH, between ca. 1.36 V (pH = 0) and 1.95 V (pH = 3). Considering a recently proposed dissolution/redeposition equilibrium,[23] the redeposition is also favourable as indicated by overpotentials of ca. 630 mV (Fig. 7). Further, complexation with anions[31–34] or electrostatic stabilization of dissolved Ir cations by the neighbouring mobile anions in the half-cell can be another reason of a reduced concentration effect in the half-cell compared to the MEA environment, in which the anions are structurally fixed. Thermodynamic predictions for favourability of redeposition by the Pourbaix diagram are strictly valid only when interaction with other ions (especially anions) in the liquid phase is negligible, as the thermodynamic calculations assume infinite dilution.[9] Regarding kinetics of re-deposition and self-reconstruction it is noted that these processes have been directly linked to the structural flexibility of oxy(hydroxide) surfaces, due to lattice oxygen participation during OER.[35]

Key observations in MEAs and half-cells and influence of confined dissolved species.—In the following, key observations and their consistency with the hypothesis of an influence of confinement of dissolved catalyst species on electrocatalytic stability will be discussed. First of all, an effect of accumulated concentration on electrocatalytic stability appears consistent with post-test analysis of PEMWE components in the literature. Agglomeration/coarsening of Ir particles occurs when dissolved Ir does not deposit where it dissolves but it is transported away and deposits preferably on larger particles. Porosity decrease/densification[4,36] has been observed. Even though, due to the unsupported catalyst structure, the particle size distribution in PEMWE is not as easily measurable as e.g. in the case of the PEM fuel cell cathodes, also in PEMWEs agglomeration within the ACL has been reported.[37–39] This effect is enhanced by the energetic favourability towards formation of larger particle sizes (Ostwald-Ripening). An "Ir band" close to the ACL/membrane interface has been observed in different studies, which is direct evidence of Ir deposition, in this case, likely related to the reduction via permeating hydrogen.[6,17] The observation of ACL thinning instead of an increase in porosity,[4,36] is comprehensible, since a concentration effect can be expected to decrease towards the boundaries of the ACL domain due to vanishing confinement of Ir species.

In the next step, two key observations (i and ii), which need to be consistently explainable by a given hypothesis about the stability-number difference between half-cells and MEA setups, will be discussed. An important observation (i) is the much higher increase of the Ir dissolution rate with a decrease of pH in the MEA setup than in the half-cell.[12,13] This can be understood considering an essential effect of the accumulation of dissolved Ir. By introducing acid electrolyte into the PEMWE anode, both the absorption competition of Ir cations with protons, as well as the coordination/complexation with electrolyte anions, will shift the absorption equilibrium to the desorption of dissolved Ir into the liquid phase. Even though the Ir equilibrium is more on the ionomer side than on the liquid side also under acidic conditions, as shown by the absorption tests with Ir-containing half-cell electrolyte solution, its shift to some extent further to the liquid phase leads to higher concentrations of Ir at the liquid side of the liquid/ionomer interface and therefore enhances the transport of Ir ions out of the catalyst layer under strong mixing conditions induced by vigorous O_2 bubbling. An extraction capability of sulfuric acid for cationic contaminants from an MEA has been reported.[30,40] One order of magnitude decrease in stability-number of MEA fed with 0.1 M $HClO_4$ was observed,[12] vs two orders with 0.1 M H_2SO_4,[13] which can be related to a higher complexation/coordination effect with sulfates than with perchlorates.[31–34,41]

(ii) Another key observation is the much larger stability-number dependence on operation time of the PEMWEs compared to half-cells.[14] A large fraction of the four orders of magnitude difference in stability-number does not occur immediately. Instead, the stability-number measured with MEAs increases substantially over time, e.g. by a factor of ca. 660 between 20 min and 11 d of operation.[13] This time dependence can certainly not be ascribed to the accumulation process of Ir ions, as the model analysis has shown that this occurs much faster. However, the observation can be explained by a distributed stability of active sites. As less stable active sites dissolve preferably, the average overall stability of the active sites increases over time. The stabilization of the structural heterogeneous active sites, related to catalyst morphology, would be expected to occur similarly in half-cell and MEA setups. However, the concentration effect in the ACL of PEMWEs leads to a more distributed stability of active sites, since some sites will experience more and others less transport confinement of dissolved Ir. For example, the vicinity of active sites either to the ionomer or the water phase, the distance to bubble transport pathways and the ACL boundaries, and the ACL porosity and tortuosity can have important influence on the confinement of dissolved Ir species and their transport. Overall, an effect of accumulation of dissolved Ir species within the ACL, which effectively leads to lower (net-) Ir dissolution rates, appears rational from a mass-transport and thermodynamic point of view and its influence is consistent with the key observations in the stability of half-cell and PEMWEs.

Essential influences in the electrocatalytic stability of PEMWE and difference to half-cells.—To explain the difference in stability-number between half-cells and MEA setup evaluated in the anode water effluent, a list of several influences shall be proposed: (A) An effect of accumulated dissolved Ir in the ACL leading to either redeposition and/or changing of the driving force of dissolution. (B) The local pH, which may differ between MEAs and half-cells can have an influence, however, likely a small one, as a decrease in stability-number by a maximum factor of 3.3 has been observed in flow-cell setups, when the electrolyte pH is varied in a wide range (1 to 7).[13] (C) Different transport directions for dissolved Ir species, which according to the previous analysis are suggested to contribute a factor of around four. (D) Kinetic/structural stabilization of active sites over time can again contribute a factor of around four (Fig. S15). Even though an effect of mobile anions on the mechanism of OER-related dissolution of Ir oxides is not commonly considered,[7,11] investigations on the difference to structurally fixed anions of solid electrolytes can provide important insights. Overall further research on the key influences, which lead to the many orders of magnitude difference in stability, seems beneficial as such understanding is essential for a rational design of the ACL to achieve a sufficient electrocatalytic stability despite low catalyst loadings. This involves the design of ACL materials but especially also a smart design of the ACL architecture, considering the interaction of the different phases inside the ACL. Understanding constraints that arise from the main mechanisms of catalyst degradation can also serve as a basis for a rational optimization of the dynamic operation under fluctuating, renewable energy sources.

Recovery of dissolved catalyst.—Due to the Ir scarcity, also recovery of Ir is an important strategy. Methods have been proposed to recover noble metals from MEAs after end of life.[42] In addition, as shown herein, also dissolved Ir in the water phase can be retrieved via absorption in anion exchange materials and regeneration with basic solutions.[43] The fraction of Ir that deposits on metal surfaces appears small (Fig. 4). Ion absorption units are typically used to prevent poisoning of the MEA from ionic impurities. A simple evaluation of the economic potential has been conducted (details in Supporting Information section 5) considering a steady-state current density of 2 A cm^{-2} and $S_{num,ch}$ of 10^9 (compare Fig. S14). With the current noble metal price, the Ir lost into the water tanks during 10 years of operation corresponds to ca. 10% of the stack costs and 2% of the overall PEMWE system cost, including large contributions of power electronics, purification, compression etc. This fraction is relatively

low because of the still low Ir prices. However, when Ir starts to restrain the application at future levels of PEMWE implementation,[1–3] the contribution of the Ir price will become large and therefore a full recovery of Ir will be of importance. Consequently, research on recovery procedures of dissolved catalyst material and their implementation can improve the economics of PEMWE in the future and enable a fully closed economic recycling of Ir.

Conclusions

The charge-related absorption affinity of Ir OER dissolution products was tested and it was analysed how the molecular charge is crucial for the transport of dissolved Ir catalyst species in PEMWE. For different Ir oxide surfaces and operating conditions, the major fraction of dissolved species in the half-cell setup is of cationic type. A constant ratio of cationic and anionic species despite different conditions, such as Ir surface type (IrOx and Ir oxide on metallic tip) and electrochemical OER dissolution procedures, is indicative of a single, dominant dissolution pathway, which is hypothesized to be related to the destabilization and rupture of the lattice structure due to lattice-oxygen participation during the OER. Particle detachment plays a negligible role in the loss of Ir in PEMWEs. In contrast to the half-cell, dissolved species in the water effluent of PEMWE anodes appear mainly in anionic form, which can be explained by the transport conditions for the dissolved Ir species within the anode catalyst layer (ACL). Cationic Ir species are absorbed in the ionomer phase of the ACL, due to their very high partition coefficient with Nafion ionomer. On the other hand, anionic Ir species are dissolved in the water phase and transported to the PTL direction, due to both migration transport and mixing effects caused by the vigorous bubbling of oxygen. This transport understanding can be used in future works for modelling and experimental validation of Ir dissolution in PEMWEs. Within this work, a model-based analysis demonstrates a strong transport confinement of Ir cations in the ACL, which leads to high accumulation of cationic Ir species within a short amount of time. It is shown that an Ir concentration effect on electrocatalytic stability, either via redeposition or by decrease of the dissolution driving force, appears rational from a mass-transport and thermodynamic point of view and consistent with key observations in the stability of Ir surfaces in half-cells and PEMWEs. Therefore, the following key influences for electrocatalytic stability of PEMWEs are suggested: (a) Effect of Ir concentration related to the ACL mass-transport conditions and the absence of mobile anions in the MEA setup. b) Ir transport direction depending on the charge of the Ir ions, which influences the stability-number assessed in the PEMWE anode water effluent. Further research on a possible direct involvement of mobile anions in the dissolution mechanism, in contrast to structurally fixed anions of solid electrolytes, can be beneficial for understanding electrocatalytic stability in PEMWE. Understanding the key influences can lead to a rational design of the electrocatalytic system and its operational optimization for the achievement of long-term durability despite low catalyst loadings. Furthermore, it is pointed out that the recovery of dissolved catalyst material not only from used CCMs but also from the anode water effluent, e.g. via the use of anion exchange materials, can improve the economics of PEMWE and enable a fully closed circular economy of Iridium.

Acknowledgments

The authors acknowledge the EU-program ERDF (European Regional Development Fund) of the German Federal State Saxony-Anhalt within the Research Center of Dynamic Systems (CDS) for financial support. Moreover, the financial support of the MaxNet Energy research consortium of the Max Planck Society is gratefully acknowledged. This work is also part of the research initiative "SmartProSys: Intelligent Process Systems for the Sustainable Production of Chemicals" funded by the Ministry for Science, Energy, Climate Protection and Environment of the State of Saxony-Anhalt.

ORCID

An Phuc Dam https://orcid.org/0000-0003-4758-9687
Georgios Papakonstantinou https://orcid.org/0000-0003-0998-0976
Kai Sundmacher https://orcid.org/0000-0003-3251-0593

References

1. S. Kiemel, T. Smolinka, F. Lehner, J. Full, A. Sauer, and R. Miehe, *Int. J. Energy Res.*, **45**, 9914 (2021).
2. U. Babic, M. Suermann, F. N. Büchi, L. Gubler, and T. J. Schmidt, *J. Electrochem. Soc.*, **164**, F387 (2017).
3. C. Minke, M. Suermann, B. Bensmann, and R. Hanke-Rauschenbach, *Int. J. Hydrogen Energy*, **46**, 23581 (2021).
4. S. M. Alia, S. Stariha, and R. L. Borup, *J. Electrochem. Soc.*, **166**, F1164 (2019).
5. R. J. Ouimet, J. R. Glenn, D. de Porcellinis, A. R. Motz, M. Carmo, and K. E. Ayers, *ACS Catal.*, **12**, 6159 (2022).
6. H. Yu, L. Bonville, J. Jankovic, and R. Maric, *Appl. Catalysis B*, **260**, 118194 (2020).
7. O. Kasian, J.-P. Grote, S. Geiger, S. Cherevko, and K. J. J. Mayrhofer, *Angew. Chem.*, **57**, 2488 (2018).
8. R. Kötz, H. Neff, and S. Stucki, *J. Electrochem. Soc.*, **131**, 72 (1984).
9. M. Pourbaix, *Atlas of Electrochemical Equilibria in Aqueous Solutions* (National Association of Corrosion Engineers, Houston, Tex.) (1974).
10. S. Cherevko, S. Geiger, O. Kasian, A. Mingers, and K. J. Mayrhofer, *J. Electroanal. Chem.*, **774**, 102 (2016).
11. S. Geiger et al., *Nat. Catal.*, **1**, 508 (2018).
12. S. Geiger, *Dissertation - Stability investigations of iridium-based catalysts towards acidic water splitting* (Ruhr-Universität Bochum) (2017).
13. J. Knöppel, M. Möckl, D. Escalera-López, K. Stojanovski, M. Bierling, T. Böhm, S. Thiele, M. Rzepka, and S. Cherevko, *Nat. Commun.*, **12**, 2231 (2021).
14. G. Papakonstantinou, I. Spanos, A. P. Dam, R. Schlögl, and K. Sundmacher, *Phys. Chem. Chem. Phys.*, **24**, 14579 (2022).
15. S. M. Alia and G. C. Anderson, *J. Electrochem. Soc.*, **166**, F282 (2019).
16. P. G. Pickup and V. I. Birss, *J. Electroanal. Chem. Interf. Electrochem.*, **220**, 83 (1987).
17. G. Papakonstantinou, G. Algara-Siller, D. Teschner, T. Vidaković-Koch, R. Schlögl, and K. Sundmacher, *Appl. Energy*, **280**, 115911 (2020).
18. S. Cherevko, S. Geiger, O. Kasian, A. Mingers, and K. J. Mayrhofer, *J. Electroanal. Chem.*, **773**, 69 (2016).
19. N. N. Greenwood, *Chemistry of The Elements* (Elsevier-Butterworth-Heinemann, Amsterdam) (2010).
20. H. Miyoshi, M. Chubachi, M. Yamagami, and T. Kataoka, *J. Chem. Eng. Data*, **37**, 120 (1992).
21. M. Ersöz and S. Yildiz, *Turk. J. Chem.*, **25**, 39 (2001).
22. D. A. Fine, *J. Inorg. Nucl. Chem.*, **32**, 2731 (1970).
23. R. Zhang, N. Dubouis, M. Ben Osman, W. Yin, M. T. Sougrati, D. A. D. Corte, D. Giaume, and A. Grimaud, *Angew. Chem.*, **58**, 4571 (2019).
24. C. Massué, X. Huang, A. Tarasov, C. Ranjan, S. Cap, and R. Schlögl, *ChemSusChem*, **10**, 1958 (2017).
25. T. Ioroi, N. Kitazawa, K. Yasuda, Y. Yamamoto, and H. Takenaka, *J. Electrochem. Soc.*, **147**, 2018 (2000).
26. A. P. Dam, G. Papakonstantinou, and K. Sundmacher, *Sci. Rep.*, **10**, 14140 (2020).
27. S. M. Alia, B. Rasimick, C. Ngo, K. C. Neyerlin, S. S. Kocha, S. Pylypenko, H. Xu, and B. S. Pivovar, *J. Electrochem. Soc.*, **163**, F3105 (2016).
28. U. Babic, M. Tarik, T. J. Schmidt, and L. Gubler, *J. Power Sources*, **451**, 227778 (2020).
29. P. Marocco, K. Sundseth, T. Aarhaug, A. Lanzini, M. Santarelli, A. O. Barnett, and M. Thomassen, *J. Power Sources*, **483**, 229179 (2021).
30. M. Zlobinski, U. Babic, M. Fikry, L. Gubler, T. J. Schmidt, and P. Boillat, *J. Electrochem. Soc.*, **167**, 144509 (2020).
31. F. A. Cotton and D. L. Weaver, *J. Am. Chem. Soc.*, **87**, 4189 (1965).
32. N. Gowda, S. B. Naikar, and G. Reddy, *Advances in Inorganic Chemistry and Radiochemistry*, **28**, 255 (1984).
33. R. A. Horne, *Nature*, **181**, 410 (1958).
34. J. Sutton, *Nature*, **169**, 71 (1952).
35. E. Fabbri et al., *Nat. Mater.*, **16**, 925 (2017).
36. M. J. Burch, K. A. Lewinski, M. I. Buckett, S. Luopa, F. Sun, E. J. Olson, and A. J. Steinbach, *J. Power Sources*, **500**, 229978 (2021).
37. S. Zhao, A. Stocks, B. Rasimick, K. More, and H. Xu, *J. Electrochem. Soc.*, **165**, F82 (2018).
38. S. M. Alia, K. S. Reeves, H. Yu, J. Park, N. Kariuki, A. J. Kropf, D. J. Myers, and D. A. Cullen, *J. Electrochem. Soc.*, **169**, 54517 (2022).
39. D. Myers, S. M. Alia, and R. Mukundan, *H2NEW Hydrogen (H2) from Next-generation Electrolyzers of Water: H2NEW LTE: Durability and AST Development* (2021).
40. S. Sun, Z. Shao, H. Yu, G. Li, and B. Yi, *J. Power Sources*, **267**, 515 (2014).
41. N. V. Abovskaya, S. A. Simanova, E. S. Boichinova, and M. K. Fedorov, *Russ. J. Appl.Chem.*, **79**, 563 (2006).
42. M. Carmo, G. P. Keeley, D. Holtz, T. Grube, M. Robinius, M. Müller, and D. Stolten, *Int. J. Hydrogen Energy*, **44**, 3450 (2019).
43. N. A. Bykovsky, E. A. Kantor, P. A. Rahman, L. N. Puchkova, and N. N. Fanakova, *IOP Conf. Ser.: Earth Environ. Sci.*, **194**, 92003 (2018).